Analysis of the 23 June 2001 M_w = 8.4 Peru underthrusting earthquake and its aftershocks

S. L. Bilek and L. J. Ruff

Department of Geological Sciences, University of Michigan, Ann Arbor, MI, USA

Received 24 May 2002; revised 4 August 2002; accepted 13 August 2002; published 19 October 2002.

[1] On 23 June 2001, a M_w = 8.4 underthrusting earthquake occurred in the southern Peru subduction zone, followed by several large aftershocks, including 26 June (M_w = 6.7) and 7 July (M_w = 7.5). Broadband analyses of seismic data for the largest of these earthquakes show southeastward rupture of 180 km along the portion of the subduction zone previously ruptured in 1868 (M_w 8.8–9). Moment release distributions determined are consistent with aftershock location patterns. Earthquake rupture mode varies along southern Peru, from larger multi-segment rupture in 1868 to several smaller segment ruptures in 2001, similar to rupture variation observed in northern Peru and other subduction zones. Based on models of subduction zone segment interaction, the 2001 earthquake sequence may suggest a shorter recurrence time for future earthquakes along this portion of the Peru-Chile subduction zone. *INDEX TERMS:* 7215 Seismology: Earthquake parameters; 7223 Seismology: Seismic hazard assessment and prediction; 7230 Seismology: Seismicity and seismotectonics. **Citation:** Bilek, S. L., and L. J. Ruff, Analysis of the 23 June 2001 M_w = 8.4 Peru underthrusting earthquake and its aftershocks, *Geophys. Res. Lett.*, *29*(20), 1960, doi:10.1029/2002GL015543, 2002.

1. Introduction

[2] Several great underthrusting earthquakes have occurred along the entire extent of the Peru margin. Earthquakes in 1604, 1687, 1746, 1868, and 1877 each ruptured segments of the margin of more than 250 km [*Nishenko*, 1991; *Swenson and Beck*, 1996]. However, studies of underthrusting earthquakes which occurred in northern and central Peru subduction segments over the past 100 years suggest changes in the mode of earthquake rupture, as earthquakes in 1940, 1942, 1966, 1974, and 1996 ruptured smaller segments of the plate margin previously broken in larger historical earthquakes [*Beck and Ruff*, 1989; *Beck and Nishenko*, 1990; *Swenson and Beck*, 1996; 1999].

[3] On 23 June 2001, a M_w 8.4 underthrusting earthquake occurred in the southern portion of the Peru subduction zone (Figure 1). This earthquake, the largest to occur worldwide in the last 25 years, produced extensive damage to several coastal towns and generated a regionally destructive tsunami. It was followed by several large aftershocks, including a M_w 7.5 aftershock on 7 July 2001.

[4] In this paper, we present source analyses of the 23 June mainshock as well as the largest aftershock of 7 July. We determine relative source time functions for these two earthquakes using surface wave data to estimate rupture direction and length. In addition, we calculate the distribution of moment release using teleseismic body waves. These two methods yield similar results, that of southeast rupture with the maximum moment release within 120 km southeast of the epicenter.

0094-8276/02/2002GL015543

2. Data Analysis

2.1. Surface Wave Empirical Green's Function Analysis

[5] We use surface waves to determine source time functions using the empirical Green's function (EGF) approach. This method has been used for many earthquake source analyses, providing accurate estimates of the source time functions for large earthquakes [e.g., *Ammon et al.*, 1993]. The method involves deconvolving surface wave recordings of a smaller earthquake (the EGF) from the surface wave recordings of the larger earthquake. In principle, this deconvolution removes wave propagation and instrument effects, yielding relative source time functions for each station. The resulting time functions are typically smooth, reflecting the frequency content limitations of the data and signal noise, masking fine-scale details. Thus, this method provides an accurate estimate of the gross features of the earthquake rupture.

[6] Similarity in earthquake parameters help ensure that the EGF deconvolution process removes all wave propagation effects. There are several aftershocks of the 23 June earthquake, however aftershocks located near the epicenter are too small to be considered, or occurred within an hour of the mainshock. Our best choice for an EGF event is a M_w 6.8 underthrusting aftershock on 26 June 2001 about 250 km to the southeast of the mainshock. The focal mechanism, magnitude, and depth of this EGF event are very similar to the mainshock, however the distance from the mainshock is less than ideal. This larger separation distance between the 2 events hampers the detection of subtle directivity effects, however the dominant source features can still be identified.

[7] The surface wave arrivals are windowed by group velocity, and the relative source time functions (RSTF) are obtained by performing a frequency domain water-level deconvolution. The RSTFs are low-passed filtered at 25 s to reduce path length and intra-rupture dispersion effects [*Velasco et al.*, 1995]. We will not detect source characteristics that are shorter than ~25 s based on the choice of filter; however, as we are using this method to obtain a gross characterization of this very large event, this limitation will not be a problem. Twenty-four stations are used, providing 42 Love and Rayleigh wave RSTF for the 23 June earthquake (Figure 2a).

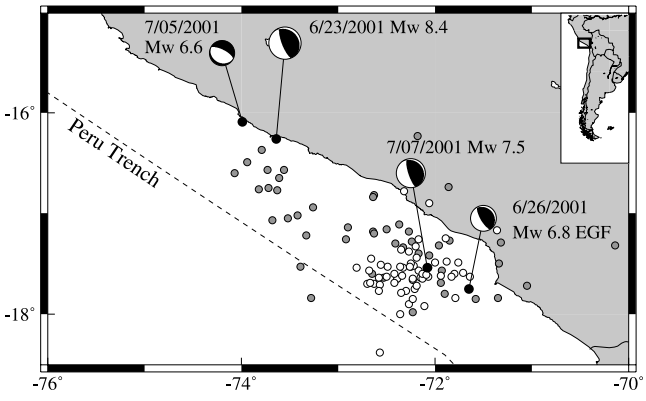

Figure 1. Map of southern Peru subduction zone. Focal mechanisms shown are from the Harvard CMT catalog. One-day aftershocks are shown for the 23 June event (gray circles) and the 7 July 2001 (white circles).

[8] Durations (t) of the relative source time functions are related to the actual source duration (t_o) and the direction of uniliateral rupture propagation (Φ_o) through a simple linear equation. We use the durations of the main pulse measured from the RSTFs to solve for source characteristics using

$$t = t_o - Xp\cos(\Phi - \Phi_o) \quad (1)$$

or

$$t = t_o - \Gamma X \quad (2)$$

where X is the length of rupture, p is the ray parameter, Φ is the azimuth to the station, and Γ is the directivity parameter. We search all possible rupture azimuths to estimate X and t_o. The actual rupture propagation direction results in the most linear fit between t and Γ. This azimuth is used to find the actual t_o and X. Durations of the main pulse width varies significantly between stations at different azimuths (different Γ). The best rupture azimuth Φ_o (116°, Figure 2b), true duration T_o and rupture length X (78 s, 138 km, Figure 2c). This suggests that this earthquake had southeast rupture of 140 km, consistent with the aftershock locations (Figure 1).

[9] We use the same technique to estimate source parameters of the 7 July earthquake, using the same EGF event as in the June earthquake case. The pulse width of the RSTFs does not change significantly with Γ, suggesting bilateral rupture for this earthquake. Using the duration measurements and all possible rupture azimuths, we can not determine a best fitting unilateral rupture model as many azimuths have equally low correlation coefficients. The overall constraint is that the rupture extent is probably less than 50 km.

2.2. Body Wave Inversion

[10] Use of body waves further constrains the details of these two earthquake ruptures. We use a P wave inversion method, e.g., *Kikuchi and Kanamori* [1982], to model the earthquake as multiple point sources along a fault plane in order to fit synthetic seismograms to the data. Focal mechanism and a trapezoidal time function are fixed parameters in the inversions. Synthetic seismograms are computed using a simple velocity model which includes a water layer, a crustal layer with v_p of 6.1 km/s over a half space with v_p of 8.0 km/s. Misfits are calculated between the synthetic and observed waveforms, with the lowest misfit providing the best estimate of moment release on the fault plane.

[11] For the June earthquake, we use 18 azimuthally well distributed teleseismic P waves in the inversion. We test all possible strikes, dips, and rakes for this event, finding a strike of 310, dip 23, rake 75, depth of 33 km, trapezoid duration of 9 s, and 10 subevents to produce the best fit of synthetic waveforms and data. We allow subevent position to vary along the strike direction, given a range of ±300 km from the epicenter with grid spacing of 10 km. The source time function determined with these inversion parameters shows most moment was released by ~90 s, with a minor subevent at ~120 s (Figure 3a), roughly consistent with the results from the surface wave analysis. The majority of the moment was released between 60–90 s. The total moment determined here (6.3×10^{21} Nm) is similar to that determined by Harvard ($\sim 5 \times 10^{21}$ Nm). Solving for subevent locations along the fault plane places the largest subevent of moment release 120 km to the SE of the epicenter, with other significant moment release occurring at the epicenter and ~160 km SE of the epicenter (Figure 3b). These results are consistent with strong unilateral rupture directivity to the southeast as suggested by the surface wave data. We also perform a 2-D inversion allowing both along strike and depth variation of subevents, finding a 2~7 km shift updip.

[12] For the 7 July aftershock, 16 stations are used in the inversion. We again tested a range of focal mechanisms, finding both the Harvard CMT mechanism and a variation (strike 296, dip 29, rake 51) producing synthetic seismo-

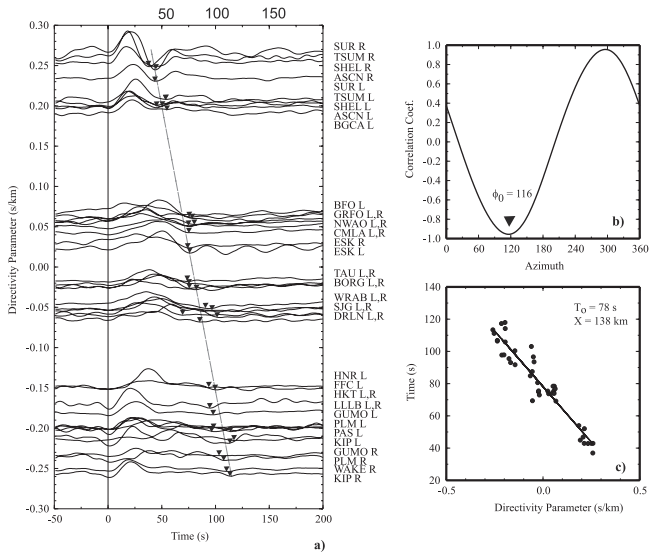

Figure 2. Surface wave directivity results for the 23 June 2001 earthquake. (a) RSTF for the June mainshock noted with station and wave type. Small triangles indicate termination for the duration pick on the RSTF. The dashed line represents duration and directivity parameter values for the best fit model to the data. (b) Results of search for the best rupture azimuth for this earthquake. Highest correlation coefficient occurred at an azimuth of 116°. (c) Duration measurements plotted with Γ. The line is the best least squares fit to the data, using a rupture azimuth of 116.

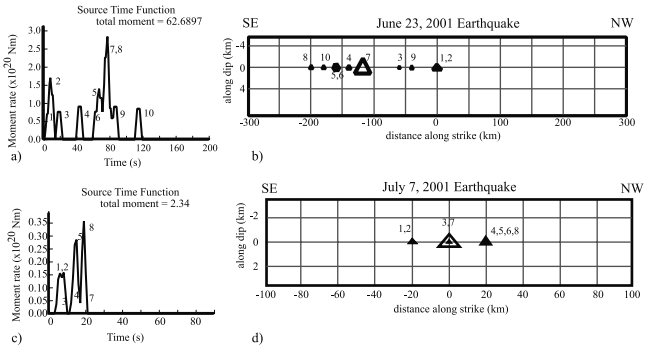

Figure 3. Body wave inversion results for the 23 June and 7 July 2001 earthquakes. (a) Source time function for the 23 June 2001 event, with the numbers reflecting the temporal order of subevents and symbol size reflecting relative subevent moment release. (b) Locations of subevents along the 23 June fault plane. Rupture began at the epicenter (0,0) and propagated to the SE. (c,d) Source time function and subevent locations for the 7 July earthquake, similar to (a,b).

grams which fit the seismograms equally well. The inversion results shown in Figure 3 use the latter mechanism, a depth of 20 km, triangle duration of 4 s, and 8 subevents. Subevents vary in the strike direction, with grid spacing of 10 km. The source time function for this earthquake has a total duration of about 20 s (Figure 3c). The total moment determined here (2.3×10^{20} Nm) is similar to that determined by Harvard (2.6×10^{20} Nm). Most of the moment was released at the epicenter (Figure 3d).

3. Aftershocks

[13] These earthquakes produced a vigorous aftershock sequence of ~450 earthquakes in the region during the 1-month period following the 23 June earthquake. The region of aftershock activity is elongated further in the southeast direction as compared to both surface wave and body wave estimates for the rupture length of the June event. There are less aftershocks in the segment we estimate as the region of main moment release. Using the full length of the aftershocks, we determine a fault area of 300 km × 100 km. Using the length determined from our inversions, we estimate 180 km × 100 km. Aftershocks between the 23 June mainshock and the 7 July aftershock generally occurred updip of the mainshock, as well as to the south of the eventual 7 July event. The cluster near the epicenter of the July earthquake likely defines the roughly circular rupture area (~50 km × 50 km) for this event, as suggested by the lack of rupture directivity seen in the surface wave or body wave analysis.

4. Summary and Implications

[14] We use aftershock areas as well as the inversion-based fault areas to estimate average displacements for these earthquakes. For the June event, we calculate average displacements of 5.0 m (full aftershock fault area) to 8.4 m (smaller fault area of concentrated moment release), using the Harvard CMT moment of 5×10^{21} Nm and rigidity of 3.3×10^{10} N/m^2. For the July event, we estimate an average displacement of 2.8 m, using a circular rupture area of 2800 km^2 from aftershocks, Harvard CMT moment of 2.6×10^{20} Nm, and rigidity of 3.3×10^{10} N/m^2. Combining both large earthquakes in the sequence suggests total average displacement of 8–11 m. Using the convergence rate of 8 to 9 cm/yr of the Nazca plate, approximately 10.5 to 12 m of tectonic displacement has accumulated in this region since the last great earthquake in 1868. This is comparable to that released during the 2001 earthquake sequence.

[15] The 23 June and 7 July earthquakes occurred in the area that ruptured during the 1868 earthquake (Figure 4). These earthquakes occurred south of the subducting Nazca Ridge, with the northern boundary of rupture corresponding roughly to the region where flat slab subduction returns to normal dipping slab subduction. The rupture area determined from our analysis and the aftershock zone end approximately 100 km northwest of the geometric corner of the coastline, and there does not appear to be any obvious

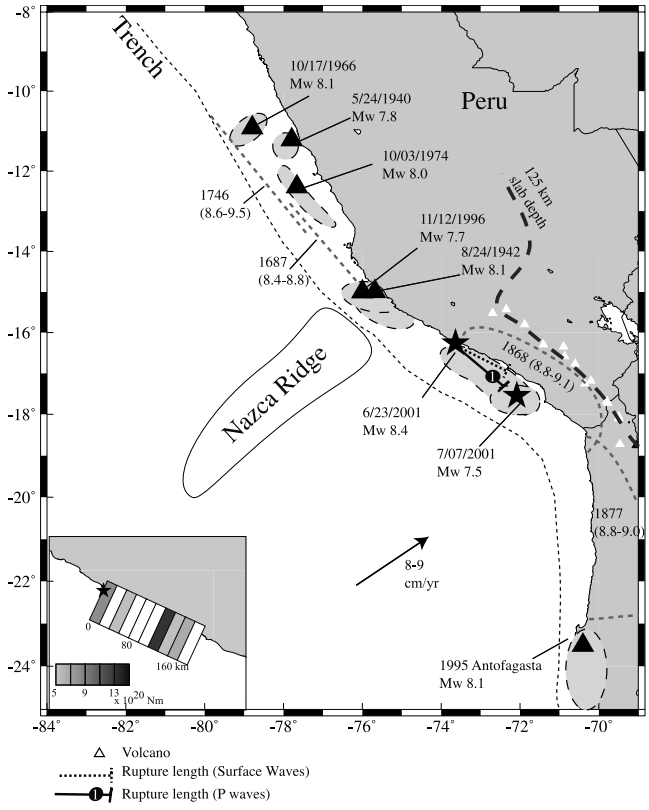

Figure 4. Map of the Peru-Chile margin. Locations of 20th century earthquakes (triangles) and corresponding rupture areas (gray ellipses) taken from *Beck and Ruff* [1989], *Swenson and Beck* [1999] (1942, 1996), and *Carlo et al.* [1999]. Estimates of rupture areas (gray, short dashed lines) for historical seismicity are from *Spence et al.* [1999]. Small triangles are locations of volcanoes of southern Peru, northern Chile [*Simkin et al.*, 1981]. Approximate position of the 125 km slab depth contour from *Cahill and Isacks* [1992]. For the 2001 earthquakes (stars), shaded gray regions denote aftershock areas. Inset, moment release distribution based on the body wave inversion, with estimates for moment release of the largest 5 subevents of Figure 3.

tectonic feature in the subducting plate to correspond with the southern termination of rupture for these earthquakes.

[16] Estimates of the rupture area and magnitude of the 1868 earthquake come from macroseismic intensity records along the Peru coast [*Comte and Pardo*, 1991]. These estimates suggest the 1868 earthquake (M_w 8.8–9.1) was significantly larger than the 2001 earthquake (M_w 8.4), with a rupture zone extending ~100+ km further southeast than the rupture extent of the 2001 earthquake sequence. The change from a M_w 8.8–9 earthquake to M_w 8.4 earthquake rupture suggests a change in the rupture mode of great earthquakes, similar to that observed for northern Peru [*Beck and Nishenko*, 1990].

[17] *Nishenko* [1991] lists a previous great earthquake in 1604 along the southern Peru margin. Intensity estimates suggest the 1604 earthquake was similar to the 1868 in size. Using these 2 great earthquakes, *Nishenko* [1991] estimates a recurrence time of 264 years for this segment. Both 2001 earthquakes were smaller magnitude than the historical great earthquakes, but occurred much sooner than expected based on the previous events (133 years instead of 264 years). *Comte and Pardo* [1991] and *Swenson and Beck* [1996] discuss other earthquakes in this segment such as the large 1784 event. Based on intensity estimates, these earthquakes were likely smaller magnitude than the 2001 earthquakes.

[18] Variation in great earthquake rupture mode has been noted in other subduction zones as well. *Ruff* [1996] observes this variable rupture mode in Ecuador-Columbia, Aleutians, and Sanriku. Each region experienced a great earthquake, followed by smaller magnitude earthquakes re-rupturing the margins with shorter than expected recurrence times. *Ruff* [1996] suggests a model of segment interaction allowing this variation from one earthquake rupturing several segments to subsequent earthquake rupture of individual segments with shorter recurrence times. The individual ruptures transferred stress to adjacent segments, causing additional earthquakes to break segments previously ruptured in the multi-segment event. The amount of interaction between the segments would be related to the strength of segment to segment coupling. With the occurrence of the 2001 earthquake sequence, the southern Peru margin can be added to the list of subduction zones where rupture mode switches for the current sequence.

[19] The idea of segment interaction leads to interesting questions concerning earthquake occurrence in the southern Peru and northern Chile subduction zone. Based on the historical intensity estimates of the 1868 rupture zone and the aftershocks and fault inversions for the 2001 earthquake sequence, gaps are suggested at the termination of the 2001 earthquake ruptures and in the region of the 1877 earthquake (Figure 4). A seismic gap at the southern termination of the 2001 earthquakes is possible based on the available information; however its location could be questioned due to possible inaccuracies in the intensity-derived rupture zones of the 1868 earthquake as well as the fact that displacements calculated for the 2001 earthquake sequence correspond to the amount of displacement accumulated since 1868. The region of the previous 1877 earthquake is more problematic. There are no good estimates of a recurrence interval for this segment as there no known earthquakes prior to 1877 [*Nishenko*, 1991]. Since 1877, roughly 10 m of tectonic displacement has accumulated in this segment using the 8–9 cm/yr convergence rate. In addition, the segment has now been bounded by 2 great earthquake ruptures, the 2001 earthquake sequence and the 1995 Antofagasta M_w 8.1 earthquake. Studies of stress triggering and loading may shed light on the possibilities for the future earthquakes of this segment.

[20] **Acknowledgments.** Data used in this study were obtained from IRIS DMC. We thank T. Melbourne, E. Norabuena, and E. Geist for helpful discussions about this earthquake. Two anonymous reviewers provided many constructive suggestions and improvements for the manuscript.

References

Ammon, C., A. Velasco, and T. Lay, Rapid estimation of rupture directivity: Application to the 1992 Landers (M_s = 7.4) and Cape Mendocino (M_s = 7.2) California earthquakes, *Geophys. Res. Lett.*, *20*, 97–100, 1993.

Beck, S. L., and L. J. Ruff, Great earthquakes and subduction along the Peru trench, *Phys. Earth Planet. Int.*, *57*, 199–224, 1989.

Beck, S. L., and S. P. Nishenko, Variations in the mode of great earthquake rupture along the Central Peru subduction zone, *Geophys. Res. Lett.*, *17*, 1969–1972, 1990.

Cahill, T., and B. L. Isacks, Seismicity and shape of the subducted Nazca plate, *J. Geophys. Res.*, *97*, 17,503–17,529, 1992.

Carlo, D. L., T. Lay, C. A. Ammon, and J. Zhang, Rupture process of the 1995 Antofagasta subduction earthquake (M_w = 8.1), *Pure Appl. Geophys.*, *154*, 677–709, 1999.

Comte, D., and M. Pardo, Reappraisal of great historical earthquakes in the northern Chile and southern Peru seismic gaps, *Natural Hazards*, *4*, 23–44, 1991.

Kikuchi, M., and H. Kanamori, Inversion of complex body waves, *Bull. Seismo. Soc. Am.*, *72*, 491–506, 1982.

Nishenko, S. P., Circum-Pacific seismic potential: 1989–1999, *Pure Appl. Geophys.*, *135*, 169–259, 1991.

Ruff, L. J., Large earthquakes in subduction zones: Segment interactions and recurrence times, *Subduction: Top to Bottom, Geophysical Monograph*, *96*, 91–104, 1996.

Simkin, T., L. Seibert, L. McClelland, D. Bridge, C. Newhall, and J. W. Latter, *Volcanoes of the World*, Smithsonian Institution, Hutchinson Ross Publishing Company, Stroudsburg, PA, p. 233, 1981.

Spence, W., C. Mendoza, E. R. Engdahl, G. L. Choy, and E. Norabuena, Seismic subduction of the Nazca Ridge as shown by the 1996–97 Peru earthquakes, *Pure Appl. Geophys.*, *154*, 753–776, 1999.

Swenson, J. L., and S. L. Beck, Historical 1942 Ecuador and 1942 Peru subduction earthquakes, and earthquake cycles along Columbia-Ecuador and Peru subduction segments, *Pure Appl. Geophys.*, *146*, 67–101, 1996.

Swenson, J. L., and S. L. Beck, Source characterizataion of the 12 November 996 M_w 7.7 Peru subduction zone earthquake, *Pure Appl. Geophys.*, *154*, 731–751, 1999.

Velasco, A. A., C. J. Ammon, and T. Lay, Source time function complexity of the great 1989 Macquarie Ridge earthquake, *J. Geophys. Res.*, *100*, 3989–4009, 1995.

S. L. Bilek and L. J. Ruff, Department of Geological Sciences, University of Michigan, Ann Arbor, MI 48109, USA. (sbilek@umich.edu; ruff@umich.edu)